# Acetylacetonate Ruthenium Nitrosyls: A Gateway to Nitric Oxide Release in Water Under Near-Infrared Excitation by Two-Photon Absorption

Pablo Labra-Vázquez, Vladyslav Mudrak, Marine Tassé, Sonia Mallet-Ladeira, Alix Sournia-Saquet, Jean-Pierre Malval, Pascal G. Lacroix, Isabelle Malfant

# Acetylacetonate Ruthenium Nitrosyls: A Gateway to Nitric Oxide Release in Water Under Near-Infrared Excitation by Two-Photon Absorption

**Pablo Labra-Vázquez[a,*], Vladyslav Mudrak[a], Marine Tassé[a], Sonia Mallet-Ladeira[a], Alix Sournia-Saquet[a], Jean-Pierre Malval[b], Pascal G. Lacroix[a,*], Isabelle Malfant[a,*]**

[a]*Laboratoire de Chimie de Coordination du CNRS, 205 route de Narbonne, F-31077, Toulouse, France.*
[b]*Institut de Science des Matériaux de Mulhouse CNRS-UMR 7361, Université de Haute Alsace, 15 rue Jean Starcky, 68057, Mulhouse, France*

*****Corresponding author. E-mail address: pab.labra@gmail.com, pascal.lacroix@lcc-toulouse.fr, isabelle.malfant@lcc-toulouse.fr*

Abstract

A fundamental challenge for phototriggered therapies is to obtain robust molecular frameworks that withstand biological media. Photoactivatable nitric oxide (NO) releasing molecules (photoNORMs) based on ruthenium nitrosyl (RuNO) complexes lie among the most studied systems due to several appealing features that make them attractive for therapeutic applications. Nevertheless, the propensity of the NO ligand to be attacked by nucleophiles frequently manifests as a significant instability in water for this class of photoNORMs. Our approach to overcome this limitation involved enhancing the Ru-NO π-backbonding to lower the electrophilicity at the NO by replacing the commonly employed 2,2'-bipyridine (bpy) ligand by an anionic, electron-rich, acetylacetonate (acac). A versatile and convenient synthetic route is developed and applied for the preparation of a large library of RuNO photoNORMs with the general formula $[RuNO(tpy)(acac)]^{2+}$ (tpy=2,2':6',2''-terpyridine). A combined theoretical and experimental analysis of the Ru-NO bonding in these complexes is presented, supported by extensive single-crystal X-Ray diffraction experiments and by topological analyses of the electron charge density by DFT. The enhanced π-backbonding, systematically evidenced by several techniques, resulted in a remarkable stability in water for these complexes, where significant NO release efficiencies were recorded. We finally demonstrate the possibility of obtaining sophisticated water-stable multipolar NO-delivery platforms that can be activated in the near-IR region by two-photon absorption (TPA), as demonstrated for an octupolar complex with a TPA cross section of 1530 GM at λ = 800 nm and for which NO photorelease was demonstrated under TPA irradiation in aqueous media.

## INTRODUCTION

Phototriggered therapies continue to attract significant research interest nowadays as they bear the opportunity to access an outstanding spatiotemporal control of drug delivery, thus reducing undesirable side effects thanks to the local activation of phototoxicity on well-localized targets such as solid tumors or wound infections.[1-6] The most recent approaches imply the use of two components that are largely innocuous while separated, but become highly toxic together.[7-8] The combination is comprised by low energy light and a photocleavable molecule that releases a cytotoxic agent. In this context, photoactivatable nitric oxide (NO) releasing molecules (photoNORMs) have attracted significant attention due to the appealing properties of the photoreleased molecule.[9] Indeed, NO is a highly lipophilic[10] radical and also perhaps the smallest drug ever delivered following this principle, two characteristics that result in near to barrierless diffusion through cell membranes,[11] allowing its rapid distribution into the tissues. Moreover, NO photorelease is oxygen-independent and thus viable in hypoxic tissues, and is capable of inducing cell death by apoptosis, which as opposed to other cell death mechanisms, is less prone to lead to an inflammatory response.

The development of photoNORMs is challenging partly due to the various physiological roles played by NO[12-14] which imply that its delivery can lead to drastically different effects depending on its concentration.[15-16] A poor photochemical response or a proclivity of the molecular structure to be altered in biological media can result in NO concentrations being low enough to induce problematic effects such as promoting cell growth and vascularization in the context of cancer therapy. Thus, efficient photoNORMs with a robust molecular structure are in high demand given their appealing potential biological applications. Our research group has been engaged in the development of photoNORMs, based on ruthenium nitrosyl complexes, that can be efficiently activated by two-photon absorption (TPA). This phenomenon offers a largely unparalleled control on drug delivery as significant responses are exclusively achieved within the focal point of a pulsed laser,[17-20] a volume typically around 30 $\mu m^3$,[21] small enough to be contained within a single eukaryotic cell. The second advantage in the use of TPA is that it allows irradiation with light sources of twice the wavelength needed under the one-photon absorption regime, thus activating the molecule using far-visible to near-IR ($\lambda$ = 600 – 1000 nm) light sources,[22] an interval known as phototherapeutic window due to the significant transparency of human tissues to these wavelengths.[23]

Different strategies have been explored in this context to access NO delivery platforms with large TPA cross sections ($\sigma_{TPA}$).[24] Most complexes incorporate ancillary tpy (2,2':6'2''-terpyridine) and bpy (2,2'-bipyridine) ligands, thus belonging to the $[RuNO(tpy)(bpy)]^{3+}$ (**bpy-RuNO**$^{3+}$) family of ruthenium nitrosyls. The most successful approach implies building highly polarizable and extended $\pi$-systems featuring significant local dipoles built up by strong electron donating and withdrawing groups, represented by fluorenyl and $[RuNO]^{3+}$ submolecular fragments, respectively. The stepwise increase of the dimensionality of the complexes has allowed an enhancement of the TPA response from $\sigma_{TPA}$ = 108 GM for a dipolar mononuclear complex[25] to $\sigma_{TPA}$ = 330 GM and $\sigma_{TPA}$ = 1600 GM for quadrupolar[26] and octupolar[27] polynuclear species, respectively. These values, recorded at $\lambda$ = 800 nm represent a remarkable increase from 3 to 16 times in the TPA response, allowing NO release to be conveniently activated by NIR excitation.

In spite of these encouraging results, **bpy-RuNO**$^{3+}$ complexes are significantly unstable in water, as a major drawback associated with the dominant triple bond character of the nitrosyl ligand that

consequently bears a strongly localized positive charge, making it highly susceptible to a nucleophilic attack by water, that efficiently converts the complex into the corresponding $[RuNO_2(tpy)(bpy)]^+$ species.[28-29] This type of electrophilic reactions is well-understood[30] and occur in water above pH > 3.00,[29] posing difficulties to potential biological applications. Other ruthenium nitrosyls are stable in water and display good photochemical responses,[31-32] but bear monodentate ligands that can be reasonably expected to participate in ligand exchange reactions in complex biological media, leading to products of unknown photoreactivity.

In this work, we address this issue following a molecular engineering approach based on enhancing the RuNO π-backbonding by replacing the neutral bpy by an anionic, electron-rich, acetylacetonate (acac) ligand. This structural modification brings additional appealing features related to the relatively robust character of acac in front of competing monodentate ligands found in biological media, as well as the fact that it is highly lipophilic[33-36] and confers a lower charge to the complex as compared to the **bpy-RuNO**$^{3+}$ family, with these two physicochemical parameters being widely acknowledged by various empirical rules[37-38] as favorable for drug permeability through biological membranes. It seems important to clarify that to the best of our knowledge, before our present contribution only one report by T. Meyer and co-workers had described the synthesis of any complex with this novel coordination sphere, i.e. $[RuNO(tpy)(acac)](PF_6)_2$ (**acac-RuNO**).[39] Nevertheless, in spite of this report having gathered significant attention, the informed synthesis has never been reproduced, the complex was not fully characterized and no photochemical investigation had been conducted. While we interestingly coincided in finding an enhanced π-backbonding caused by the introduction of an acac ligand, some differences regarding the informed electrochemical and optical absorption features of this complex were found.

The discussion of the manuscript is centered on three main axes: (1) presenting the development of an improved general scope synthetic route for the novel coordination sphere; (2) systematically showcasing the impact of the bpy→acac ligand replacement on the geometry and the electronic, photophysical, redox and photochemical properties of the complex–and (3) demonstrating the possibility of developing a water-stable ruthenium nitrosyl capable of NO release within the phototherapeutic window triggered by an efficient TPA response.

## RESULTS AND DISCUSSION

### Synthesis and characterization

Different synthetic routes, summarized in Scheme 1, were screened from tpy (**1a**) targeting complex $[Ru^{II}NO(tpy)(acac)](PF_6)_2$ (**6a**, **acac-RuNO**). While intermediates **2a** and **3a** were flawlessly prepared following reported methodologies,[32, 40] the next steps proved unexpectedly difficult when compared to the synthesis of structurally related ruthenium nitrosyls of the **bpy-RuNO**$^{3+}$ family.[24, 26] Most of these difficulties arose from the remarkably lower lability of the chlorido ligand in **3a** when compared to its homologous complex $[Ru^{II}Cl(tpy)(bpy)](PF_6)$, which swiftly undergoes the needed $Cl \rightarrow NO_2$ substitution that we found inoperative for the direct **3a**→**5a** conversion. The reported synthesis of **6a** by T. Meyer and co-workers[39] proposes the use of $[Ru^{II}(H_2O)(tpy)(acac)](PF_6)$ as it bears a more labile aqua ligand. We were unfortunately unable to extend the synthesis of the aqua solvate[41] for other complexes due to significant problems of solubility in water when attempting this

reaction using 4'-aryl substituted terpyridyl ligands. Our approach was to employ the acetonitrile solvate **4a** instead, being conveniently prepared following the methodology reported by C. Turro and co-workers.[40] This alternative synthetic intermediate gratifyingly underwent the desired ligand exchange towards **5a** yielding analytically pure **6a** after acid treatment. Further simplification of the synthetic route was attempted through the direct transformation of **4a** into **6a** by treatment with $NOBF_4$, a popular nitrosylating agent. As discussed in the Supplementary Information (Section S3), this led to three unexpected products, one of which was nitrated at the acac ligand. It must be remarked that nitration was also observed during photolysis (*vide infra*), thus evidencing a high proclivity of these complexes towards electrophilic substitution at this position

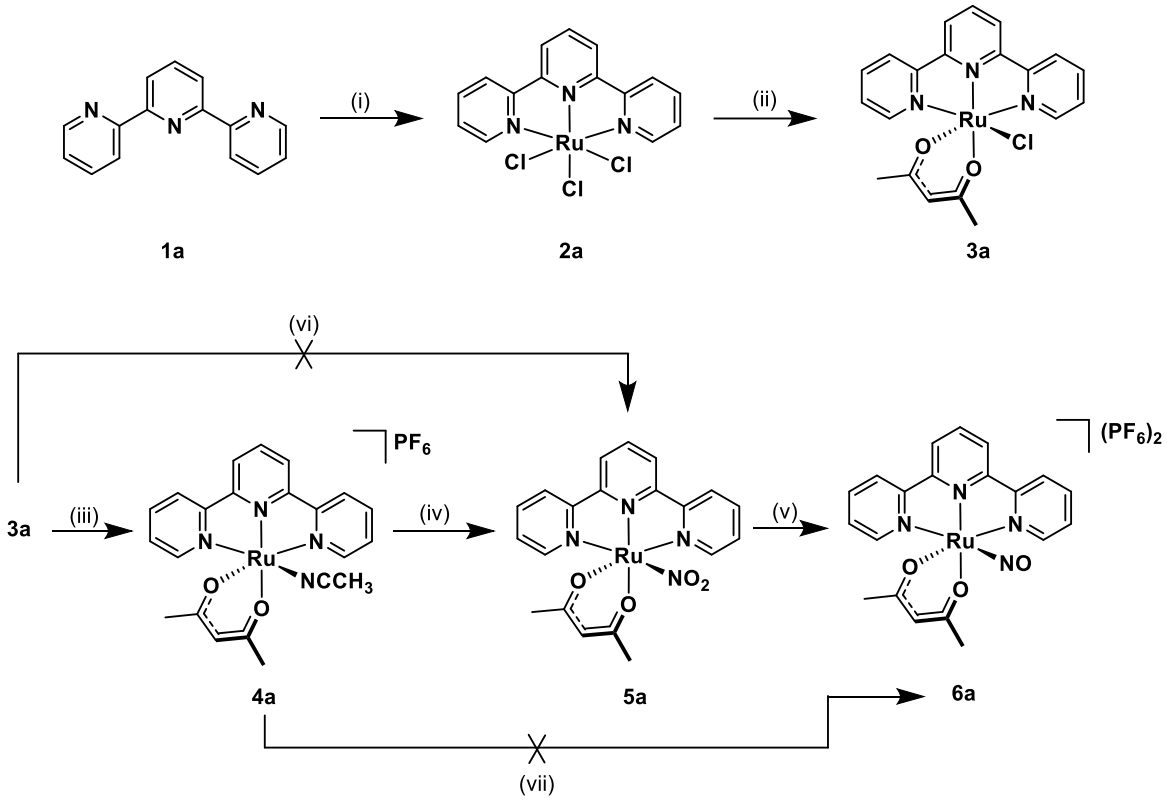


**Scheme 1.** Different synthetic routes explored for the obtention of the target $[Ru^{II}NO(tpy)(acac)](PF_6)_2$ complex. Reagents and conditions: (i) $RuCl_3xH_2O$, EtOH, reflux (88 %); (ii) acetylacetone, LiCl, $Et_3N$, $EtOH/H_2O$, reflux (89 %); (iii) $CH_3CN/H_2O$, reflux, then $NH_4PF_6$ (> 99 %); (iv) $NaNO_2$, $EtOH/H_2O$, reflux (91 %); (v) $HCl/H_2O$, rt, then $NH_4PF_6$ (66 %); (vi) $NaNO_2$, $EtOH/H_2O$, reflux; (vii) $NOBF_4$, $CH_3CN$, rt.

We decided to explore the ligand scope of this synthetic route on a large group of terpyridyl ligands to gain information on (a) the tolerability of functional groups and heterocycles with a rich synthetic and coordination chemistry, as they can potentially allow further functionalization or anchoring to macromolecules or nanostructures and (b) the influence of different electron donating/withdrawing effects on the optical and photochemical properties of the studied ruthenium nitrosyl complexes. As shown in Scheme 2, the synthetic route turned out very versatile, allowing the obtention of a large library of ruthenium nitrosyls bearing a diversity of interesting functional groups with diverse electron withdrawing and donating effects. The global yields (24 to 66 %) were excellent considering the number of steps, the complexity of the molecules and the fact that no purification

procedure was needed at any step.[42] It should be noticed that the outcome for the last synthetic step for the aminophenyl derivatives was complex; as for the 4-dimethylaminophenyl derivative, two different ruthenium nitrosyls, **6f** and **6f'**, were isolated, corresponding to the non-protonated (2+) and protonated (3+) species, respectively, while for the diethylaminophenyl analogue only the protonated species (**6g'**) was obtained.

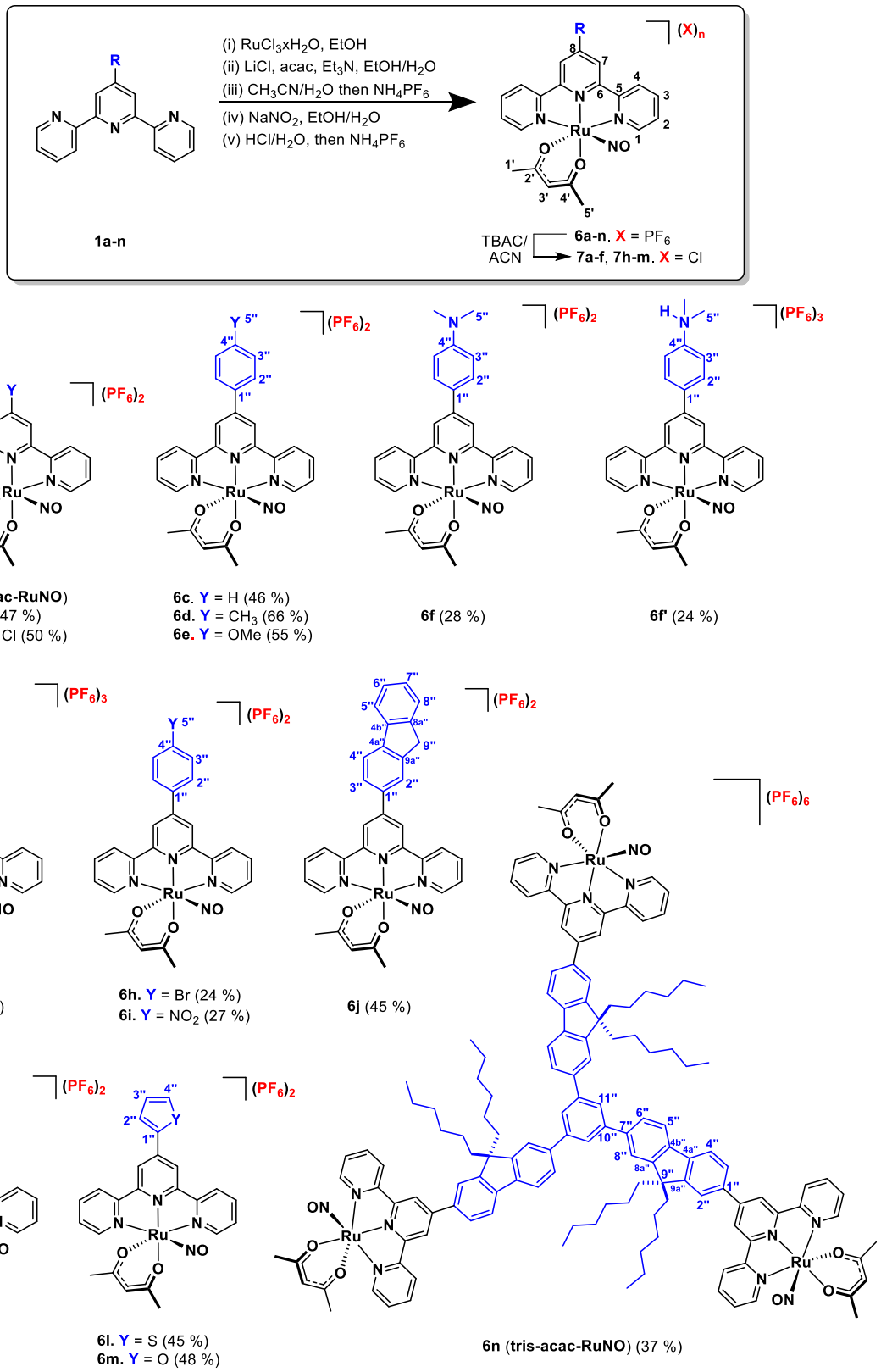


**Scheme 2.** Ligand scope in the synthesis of ruthenium nitrosyl complexes **6a-n** (5-steps yields in parentheses) and subsequent metathesis to water soluble **7a-f** and **7h-m**.

The developed synthetic strategy was satisfactorily extrapolated to the preparation of the targeted star-shaped complex **tris-acac-RuNO** (**6n**) from the corresponding tris-terpyridyl ligand (**1n**) obtained through an efficient triple Suzuki cross-coupling reaction (for details see the Supporting Information, Section S2). The identity of all the final ruthenium nitrosyl complexes was stablished using multinuclear 1D and 2D (COSY, NOESY, HSQC, HMBC) NMR, IR spectroscopy, HRMS and elemental analyses (details are gathered in the Supporting Information). Interestingly, the nitrosyl ligand was systematically detected both as a radical and as a cationic ligand in the HRMS analyses of these complexes, as exemplified in the Supporting Information (Figures S133-S134). Nevertheless, as discussed below, both single-crystal X-Ray diffraction (SXRD) analyses and IR spectroscopy proved this observation to be an artifact from the HRMS analyses, as the nitrosyl ligand in these complexes was unambiguously confirmed to be coordinated as the $NO^+$ cation, with νNO frequencies in the 1882 - 1922 $cm^{-1}$ interval and an almost linear coordination of the nitrosyl with Ru-NO angles close to 180 °.

As shown in Supplementary Figure S132, analysis of the NMR for the phenyl-substituted series revealed the marked charge-transfer effects occurring within these complexes in the ground state; electron density is polarized from the phenyl rings towards the strongly withdrawing nitrosonium cation. The effect is clearly observed for H-7 and H-3'', on which the resonance hybrid for the charge-transfer process bears partial negative charges of increasing significance (along with an increasing magnetic shielding) as the donating capabilities of the substituent in the phenyl ring increases. This tendency correlates well with the $\sigma_P^+$ Hammett constant of the different substituents,[43] corroborating the relationship between the charge transfer capabilities of the R substituents with the magnetic shielding of these nuclei.

Finally, with the aim of increasing their solubility in water, we performed a $PF_6 \rightarrow Cl$ metathesis reaction on all the obtained $[Ru^{II}NO(R\text{-}tpy)(acac)](PF_6)_2$ complexes using tetrabutylammonium chloride (TBAC); complexes **6a-6f** and **6h-6m** satisfactorily yielded the expected $[Ru^{II}NO(R\text{-}tpy)(acac)](Cl)_2$ species (**7a-f**, **7h-m**), whilst we were unable to obtain the corresponding derivatives for **6g'** and **tris-acac-RuNO** (**6n**) due to solubility issues; on the other hand, **6f** and **6f'** yielded the same deprotonated species $[Ru^{II}NO(4\text{-}NMe_2Ph\text{-}tpy)(acac)](Cl)_2$ (**7f**) regardless of the starting complex.

**Structural Characterization**

As a first approach to unveiling the implications of the bpy→acac replacement on the electronic structure of these complexes, here we focus on presenting a structural characterization of **acac-RuNO** and **bpy-RuNO** as model compounds. As previously discussed, the introduction of an electron-rich anionic ligand should bring an enhancement of the Ru-NO π-backbonding as a phenomenon with the dual role of strengthening and weakening the Ru-N and N-O bonds, respectively. The weakening of the NO bond is associated with the polarization of electrons into π* orbitals of the nitrosyl, lowering its triple bond character and its positive charge, rendering it less prone to nucleophilic attacks and consequently more stable in water.

With vibrational frequencies being proportional to bond orders, one of the most convenient manners to address the modulation of Ru-NO π-backbonding in metal nitrosyls is IR spectroscopy. While there are largely separated spectral regions for the νNO stretch frequency associated with the different coordination modes of this non-innocent ligand, more subtle changes as those expected here can also be studied. In the present case, the higher Ru-NO π-backbonding in **acac-RuNO** was evidenced with νNO = 1907 $cm^{-1}$ being indeed significantly lower than the reported value for **bpy-RuNO** (νNO = 1940 $cm^{-1}$)[44]; a similarly large difference was also observed when comparing scaled[45] analytical frequency computations at the B3PW91/6-31G* level *in vacuo* for both species, with νNO = 1956 and 1974 $cm^{-1}$ for the **acac-RuNO**$^{2+}$ and **bpy-RuNO**$^{3+}$ cations, respectively, thus discarding the possibility of the experimental difference stemming from solid-state effects. As shown in Table S6, these observations are extended to all the investigated acetylacetonate ruthenium nitrosyl complexes, with experimental νNO frequencies in the 1882 - 1922 $cm^{-1}$ interval. These values are in good agreement with a $Ru^{II}(NO^{+})$ configuration for this family of complexes and indicate an enhanced Ru-NO π-backbonding in comparison with **bpy-RuNO**.

Structural data can provide further valuable evidence on the occurrence of this phenomenon, expected to manifest as a bending the Ru-NO ligand and a modification of the Ru-N and N-O bond lengths, that should be shortened and lengthened, respectively. While SXRD data for **bpy-RuNO** had been informed by our group,[46] no crystallographic data was available for **acac-RuNO**; crystals of this complex were consequently grown by slow diffusion of diethyl ether into saturated acetonitrile solutions and the resulting crystalline sample was analyzed by SXRD (further details are contained as Supporting Information, Section S4). The asymmetric unit of **acac-RuNO** contains two independent **acac-RuNO**$^{2+}$ cations (one of which is disordered over two independent positions) and four $PF_6^-$ anions, confirming the oxidation state of the metal with a $\{Ru\text{-}NO\}^6$ electronic configuration in the Enemark-Feltham notation.[47] These results provide a nonambiguous confirmation for the $Ru^{II}(NO^{+})$ configuration found by IR spectroscopy as discussed above. Similar features are found for **bpy-RuNO** which shares a $Ru^{II}(NO^{+})$ configuration and has two independent **bpy-RuNO**$^{3+}$ cations in its asymmetric unit.

The crystal structure of both complexes is illustrated in Figure 1, showing one of the conformers found in their asymmetric units (further details in the Supporting Information, Figures S2 and S3). As it can be seen, the octahedral symmetry is less distorted for **acac-RuNO** due to the larger bite angle of the acac ligand, resembling previous observations on this ligand substitution by C. Turro and co-workers.[40] Regarding the Ru-NO fragment, the observed interatomic distances and angles confirmed the expected tendencies, with Ru1-N1 and N1-O1 distances being comparatively shorter and longer, respectively, for **acac-RuNO**, which also displayed a slightly more bent nitrosyl ligand as indicated by its lower Ru1-N1-O1 angle when compared to **bpy-RuNO**. Although the differences are rather modest and thus indicative of a dominant triple bond character for the nitrosyl ligand in both complexes, they are anyways in good agreement with our expectations associated with a higher Ru-NO π-backbonding in **acac-RuNO**.

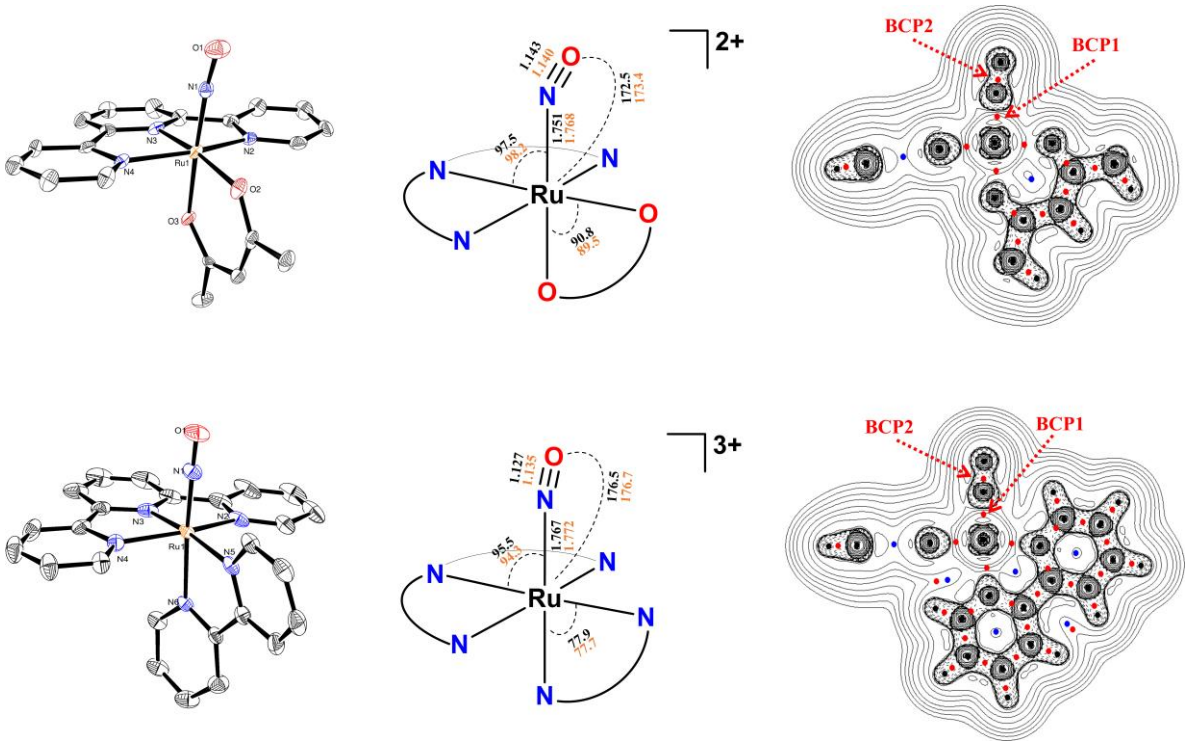


**Figure 1.** Structural differences between the coordination spheres in **acac-RuNO**$^{2+}$ (**6a**$^{2+}$) (top) and **bpy-RuNO**$^{3+}$ (bottom) as observed in their asymmetric units (left) and in gas-phase DFT-optimized (B3PW91/6-31G*) conformations; relevant interatomic distances (in Å) and angles (in deg) are summarized in the middle with SXRD and DFT values shown in black and orange, respectively. Contour diagrams of the Laplacian distribution of electron density, $\nabla^2\rho(r)$, along the N3-Ru1-O3(N6) plane are shown in the right as computed from the DFT-optimized geometries; relevant bond critical points (BCP) along the Ru1-N1 (BCP1) and N1-O1 (BCP2) bond paths are signaled with arrows. SXRD values are averages of the different conformers found in the asymmetric units. Thermal ellipsoids are drawn at 50 % probability; counterions, solvent molecules and hydrogen atoms are omitted for clarity. SXRD data for **bpy-RuNO** was previously reported elsewhere (CCDC: 1992867).[46]

To verify that the observed geometric differences did not stem from crystal packing effects, the DFT-optimized conformations of these complexes in vacuum were also inspected (for details see the Supporting Information, Section S6); relevant geometrical parameters, also shown in Figure 1, gratifyingly agreed with the observed experimental tendencies. To gain further insight on this matter, topological analyses of the electronic charge density, $\rho(r)$, and its Laplacian, $\nabla^2\rho(r)$, were carried out within the framework of Bader's Quantum Theory of Atoms-in-Molecules (QTAIM),[48-49] a rigorous method employed in the study of covalent and non-covalent interactions;[50-52] the data for relevant bond critical points (BCP) lying along the Ru-NO (BCP1) and N-O (BCP2) bond paths, are gathered in Table 1, where low positive values of $\nabla^2\rho(r)$ at BCP1 are in good agreement with the Ru-NO bond lying in between a covalent and a closed-shell interaction, whereas negative values at BCP2 reflect the covalent nature of the N-O bond; perhaps the most important information from these analyses are the differences in $\rho(r)$ for both complexes at these BCPs, as electron density at the BCP correlates with bond strengths; the obtained values indeed show that the Ru-NO and N-O bonds are stronger

and weaker, respectively, for **acac-RuNO**, as expected; moreover, the low ellipticity (ε) at BCP2 for both complexes is indicative of a cylindrical distribution of electron density around the N-O axis, resembling related linear ruthenium[53] and iron[54] nitrosyls and depicting a dominant triple bond character; it should be noted however that ε at this BCP is ca. 8 times higher for **acac-RuNO** evidencing the slight deviation of the nitrosyl from the triple bond character as a consequence of the stronger Ru-NO π-backbonding.

**Table 1**. QTAIM electronic density properties at relevant bond critical points (BCP) for **acac-RuNO$^{2+}$** (**6a$^{2+}$**) and **bpy-RuNO$^{3+}$** (B3PW91/6-31G*, see Figure 1 for labeling).

| | | $\rho$(r), eÅ$^{-3}$ | $\nabla^2\rho$(r), eÅ$^{-5}$ | ε, a.u. |
|---|---|---|---|---|
| BCP1 | **acac-RuNO$^{2+}$** | 0.1813 | 0.1098 | 0.0770 |
| | **bpy-RuNO$^{3+}$** | 0.1793 | 0.1142 | 0.0013 |
| BCP2 | **acac-RuNO$^{2+}$** | 0.5990 | -0.1911 | 0.0008 |
| | **bpy-RuNO$^{3+}$** | 0.6105 | -0.2021 | 0.0001 |

To investigate if the structural features of **acac-RuNO** extended to other acetylacetonate ruthenium nitrosyls, crystalline samples for several other mononuclear complexes were obtained and analyzed by SXRD. The asymmetric units, depicted in Figure 2 showed a general agreement with the observations made above for **acac-RuNO**, with a $Ru^{II}(NO^{+})$ configuration being unambiguously confirmed in every case. While the interatomic distances and angles for the RuNO submolecular fragment in these complexes followed our previous comparative analysis with **bpy-RuNO**, no clear correlations between these geometrical descriptors and the electron donor/acceptor character of the substituents on the terpyridyl ligand were found. The fact that these anticipated correlations were not observed was accounted to crystal packing effects, as a reasonable assumption considering that NMR (discussed above) and IR/UV-Vis (discussed below) spectroscopies evidenced a clear modulation of the electronic properties of the ground-state of these complexes with the charge transfer capabilities of the terpyridyl ligand.

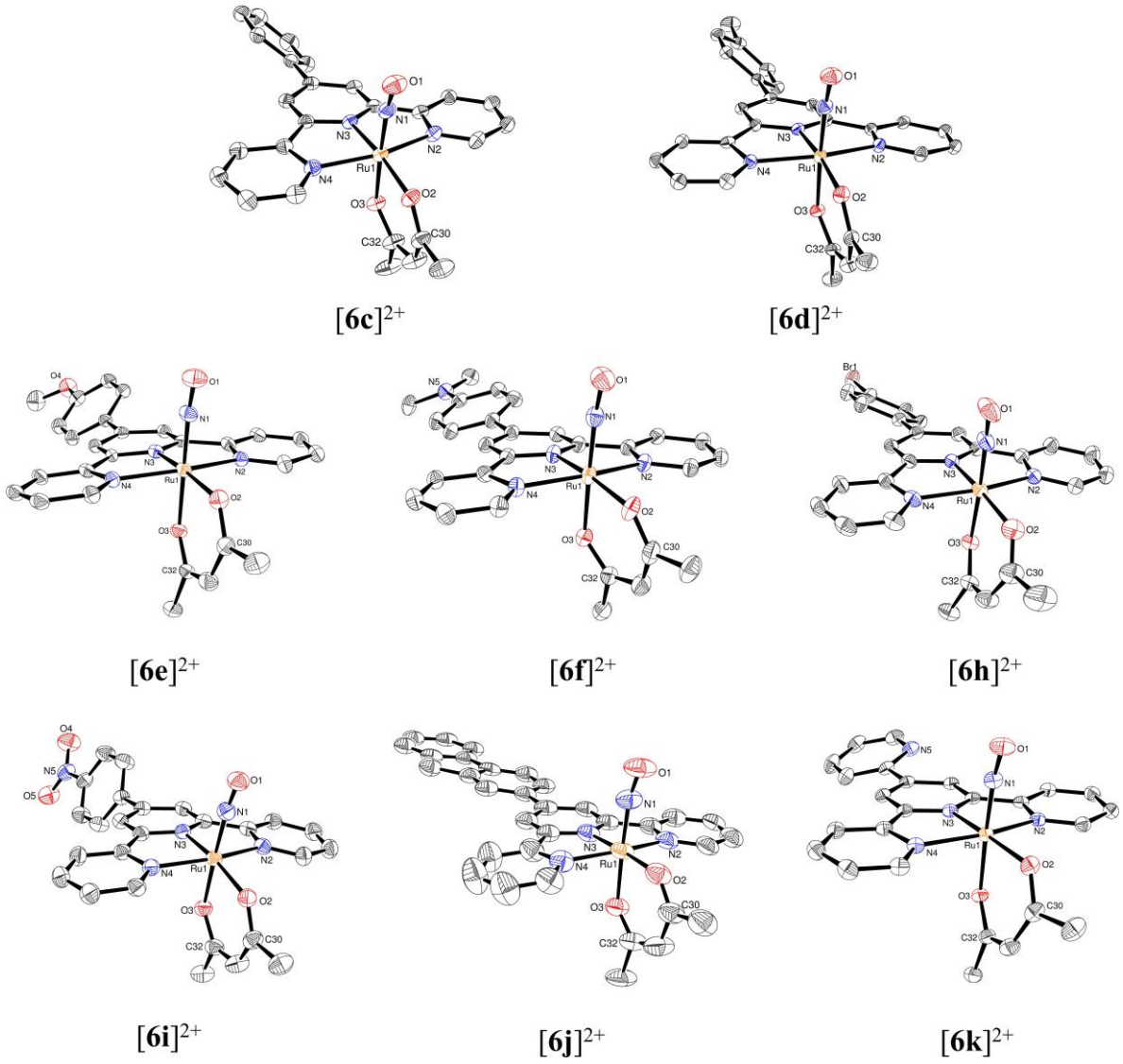


**Figure 2.** Molecular structure of ruthenium nitrosyl complexes **6c-f** and **6h-k**. Hexafluorophosphate counterions and hydrogen atoms are omitted for clarity. Thermal ellipsoids are drawn at 50 % probability.

In summary, the structural analyses presented here demonstrate that replacing the neutral bpy for an anionic acac ligand leads to an enhanced Ru-NO π-backbonding in the acac complexes. While concurring evidence indicates the presence of a nitrosyl ligand with a triple bond character and a positive charge in both types of complexes, in the acac derivatives both characteristics are slightly reduced when compared to **bpy-RuNO**. As it will be discussed in detail in the next sections, this structural modification has important consequences in the water stability and in the optical and photochemical properties of these complexes.

**Optical Characterization**

In this Section we start by analyzing the differences in the electronic and optical properties brought by the bidentate bpy→acac ligand replacement using **bpy-RuNO** and **acac-RuNO** as model compounds. This is followed by a general discussion of the optical spectra of all the different mononuclear ruthenium nitrosyl complexes developed in this work. The linear and nonlinear optical absorption properties of **tris-acac-RuNO** are discussed later in the manuscript. It seems important to clarify that, in line with the objectives of this work and in contrast to **bpy-RuNO** which reacts rapidly with water, we found **acac-RuNO** to be stable in water during considerable periods of time as evidenced by NMR spectroscopy (see the Supporting Information, Figure S137). This appealing feature is directly related to the lower charge in the NO ligand that makes **acac-RuNO** less susceptible to nucleophilic attacks.

Due to their divergent stabilities in water, the study of the optical absorption profiles of **acac-RuNO** and **bpy-RuNO** was performed in acetonitrile with support from TD-DFT computations at the CAM-B3LYP/6-31G* level. As shown in Figure 3, these complexes display similar absorption profiles, with the RuNO band (transitions 1→8 and 1→7 respectively) having a dominant tpy→RuNO character in both cases, yet with a slight (ca. 10 nm) blueshift for **acac-RuNO**, with a broad absorption around $\lambda$ = 342 nm associated with a ~0.11 eV energy gap difference for the involved dominant excitations (HOMO-1→LUMO for **acac-RuNO** and HOMO→LUMO for **bpy-RuNO**). In spite of these similarities, a remarkable feature of **acac-RuNO** is the participation of the acac ligand in the charge transfer towards the nitrosyl observed not only as a significant (16 %) contribution to the 1→8 transition but also giving rise to a new absorption band experimentally observed around $\lambda$ = 490 nm accounted to the 1→3 transition with a pure acac→RuNO character. In spite that this transition involves the population of molecular orbitals with strong Ru-NO antibonding character, irradiation at this band did not produce any noticeable NO release, which can be tentatively accounted its very low intensity.

It should be noted that analogous transitions of dominant bpy→RuNO character are predicted by TD-DFT for **bpy-RuNO** at similarly low energies, but their oscillator strengths are much weaker when compared to the RuNO band, and thus they are not experimentally observed. Indeed, participation of the bpy ligand in charge transfer towards the RuNO submolecular fragment has only been observed for a complex with strong electron-donating groups attached to the bipyridine ligand.[55] This new transition for **acac-RuNO** was observed ubiquitously for all the acac ruthenium nitrosyls both experimentally and computationally; in spite of its low intensity, this low-energy absorbance explains the pale pink/red to brown color observed for these complexes, in contrast to their bpy counterparts which are usually yellow. These observations arise as a discrepancy to the paper by T. Meyer and co-workers where a yellow color for **acac-RuNO** was informed.[39]

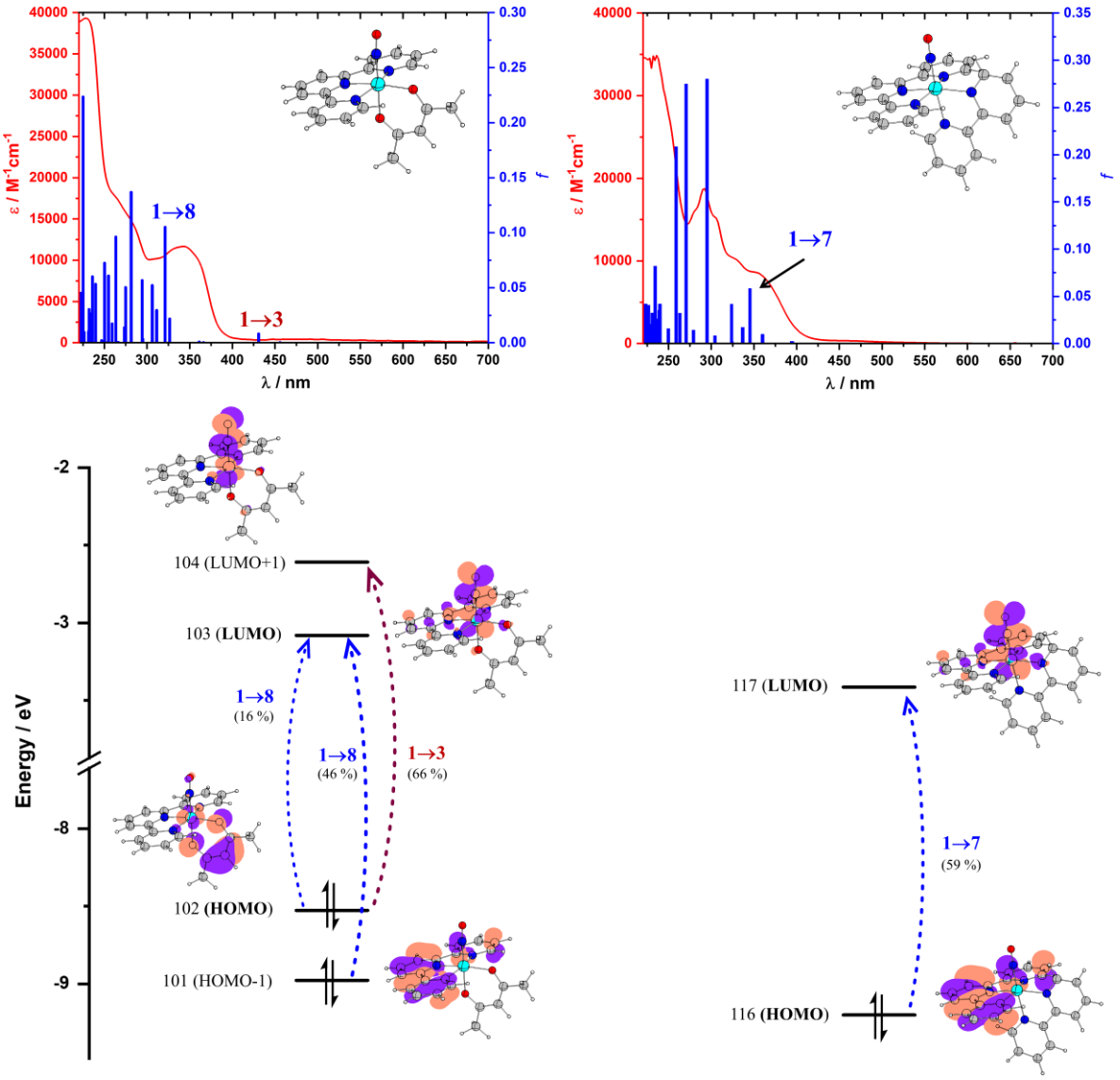


**Figure 3.** Experimental UV-Vis absorption spectra in acetonitrile for **acac-RuNO** (**6a**, top left) and **bpy-RuNO** (top right) with electronic transitions from TD-DFT computations (CAM-B3LYP/6-31*). A molecular orbital energy diagram is shown in the bottom with excitation contributions for the selected transitions.

The marked participation of the acac ligand in the charge transfer towards the RuNO fragment is also evidenced by a significant stabilization of about 0.33 eV of the LUMO level in **acac-RuNO** when compared to **bpy-RuNO**, according to the TD-DFT computations. This is accounted to a reduction of the overall charge in this submolecular fragment as a clear manifestation of the enhanced Ru-NO π-backbonding in **acac-RuNO**. This observation was corroborated experimentally by cyclic voltammetry (CV); the CV of **bpy-RuNO** and **acac-RuNO** in acetonitrile (Supplementary Figure Figure S4) exhibited two electrochemical processes attributed at two NO-centered reductions. The first reduction ($E$ = 0.42 and 0.11 V/SCE for **bpy-RuNO** and **acac-RuNO)** is reversible and attributed to the pair $Ru^{II}$-$NO^{+}$/$Ru^{II}$-$NO^{0}$ while the more cathodic one is quasi reversible occurring at -0.52 and

-0.20 V/SCE for **bpy-RuNO** and **acac-RuNO** corresponding to the pair $Ru^{II}$-$NO^0$/$Ru^{II}$-$NO^{\cdot}$.[56] For the first process, the reduction of **bpy-RuNO** (0.42 V/SCE) is easier than that of **acac-RuNO** (0.10 V/SCE). In this coordinating solvent, the behavior of the two complexes is slightly different. The irreversibility of the second reduction for the compound **acacRuNO** is attributed to the loss of the NO ligand and the coordination of a solvent molecule. This is confirmed by the voltammogram of **acacRuNO** in dichloromethane which is included as Supplementary Information (Figure S5). If the half-wave potentials of **acacRuNO** in dichloromethane ($E_{1/2}$ = 0.07 and -0.62 V/SCE) are close to those found by T. Meyer and co-workers ($E_{1/2}$ = 0.02 and -0.75 V/SCE)[39] with similar experimental conditions (same solvent, different electrolyte), on the other hand in our study the second reduction is always reversible.

After the comparison between **bpy-RuNO** and **acac-RuNO** in acetonitrile, here we study the optical properties of the obtained acac complexes in water, in connection with the intended biological applications for this class of compounds. As mentioned earlier, several mononuclear RuNO complexes were conveniently transformed into their chloride salts (**7a-f** and **7h-m**) which displayed an increased solubility in water, As depicted in Figure 4a, these complexes show UV-Vis spectra of varying complexity depending on the different substituents placed on the terpyridyl ligand, bringing absorption bands at high energy associated to ligand-ligand charge transfer transitions that cannot contribute to the NO release process.[32, 57-59] Therefore, they will not be analyzed here. The origin of the low-energy transitions was investigated by TD-DFT at the CAM-B3LYP/6-31G* level (details in the Supporting Information, Table S4 and Figures S6-S17).

The optical absorption at low energies for these complexes in water follows our previous observations for **acac-RuNO** in acetonitrile, with two main transitions being systematically observed at low energy. The first is the NO band, experimentally observed in the $\lambda$ = 323 – 514 nm interval with a high intensity ($\varepsilon$ = 8710 – 27640 $M^{-1}cm^{-1}$) and extending over a broad range of wavelengths in the form of shoulders with the main transitions having a dominant tpy→RuNO character with a moderate contribution of acac→RuNO excitations. The second band is located around $\lambda$ = 500 nm with a very low intensity ($\varepsilon$ = 260 – 1000 $M^{-1}cm^{-1}$) but not observed experimentally in **7e**, **7f**, and **7j**, due to the overlap with red-shifted transitions when a donor fragment is present on the terpyridine. As discussed previously, this accounts for acac→NO charge transfers without the involvement of any other submolecular fragment.

In parallel to our previous discussions on the modulation of the magnetic shielding of certain nuclei with the charge transfer capabilities of the ligands, here we analyze its effects on the overall optical properties of the complexes. In Figure 4b the absorption maxima ($\lambda_{max}$) of the dominant R-phenyl→RuNO based transitions are drawn against the Hammett constant, $\sigma_P^+$,[43] of the substituents on the phenyl ring. Clearly, the presence of donors leads to a reduction of the transition energy. The effects of the charge transfer capabilities on the optical absorption properties within the phenyl-substituted series associated with an increase of the energy of the occupied R-phenyl based orbital dominant in the contribution of the transition when the donating capability of R is more pronounced; as the unoccupied level is invariably described by the RuNO orbitals, the energy of which is constant all over the series, the resulting energy transition is consequently reduced as the donating character of the substituent increases (details in the Supporting Information, Figure S18).

Similarly, the computed infrared *ν*NO frequencies, also presented in Figure 4b, show a clear trend for reduced frequency in the presence of strong electron donors, capable to increase the electron density in the $\pi^*$ antibonding orbitals of the strongly withdrawing NO ligand, thus decreasing the bond order and hence the *ν*NO frequency. No clear trends were observed for experimental IR data, presented before, which was accounted to solid-state effects. Nevertheless, the values for the **acac-RuNO** series are systematically lower than those of the parent bpy complex, indicating the stability of **acac-RuNO** in water, more precisely the unlikely transformation to the $Ru^{II}$-$NO_2$ species**.**

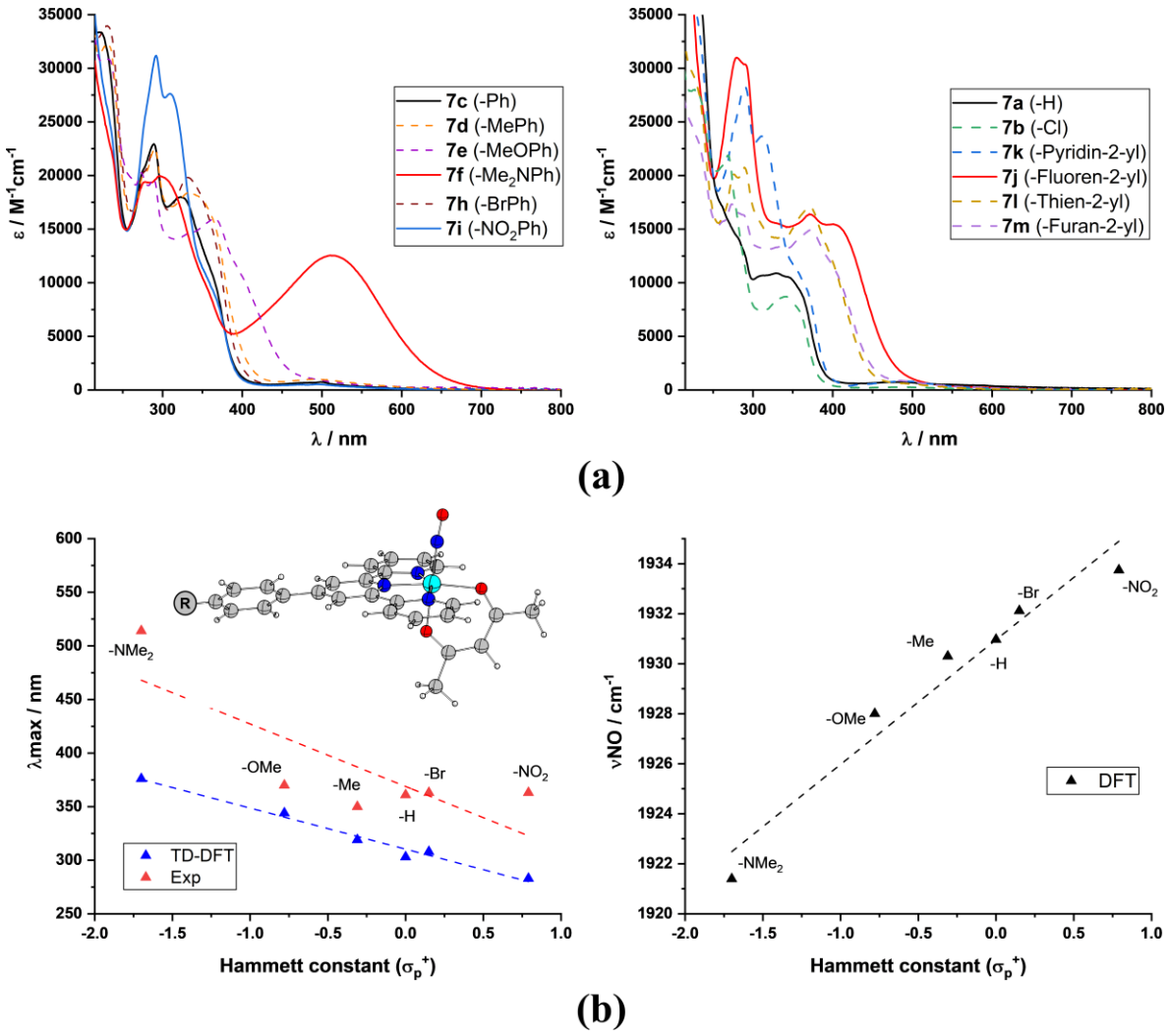


**Figure 4.** (a) UV-Visible absorption spectra for mononuclear ruthenium nitrosyl complexes in water and (b) observed variation of the experimental and TD-DFT (CAM-B3LYP/6-31G*) or DFT (B3PW91/6-31G*, scaled[45]) computed absorption maximum in water and νNO stretch frequency with the Hammett constant[43] of the substituents on the phenyl ring in the $[RuNO(R\text{-}Phtpy)(acac)]^{2+}$ series with R = $NMe_2$, OMe, Me, H, Br, $NO_2$. Discontinuous lines are linear fittings with $R^2$ = 0.636 – 0.982.

**NO Photorelease**

Having gained a detailed understanding of the electronic and optical properties of the different complexes under investigation, we turned our attention to their NO-photorelease capabilities. As highlighted in the next Section devoted to the properties of **tris-acac-RuNO**, the final goal of this work was to bring efficient TPA-triggered NO release closer to practical, biological applications. Thus, we decided to conduct most of photochemical investigations in water. Nevertheless, keeping consistency with our previous discussions and aiming at correlating the electronic and structural differences between **acac-RuNO** and **bpy-RuNO** with their photoreactivity, a comparison of these complexes is presented in acetonitrile due to the instability of **bpy-RuNO** in water.

The spectral evolution of **bpy-RuNO** under irradiation at $\lambda$ = 365 nm was previously studied by our group. The compound showed a clean transformation to the acetonitrile solvate $[Ru(tpy)(bpy)(CH_3CN)]^{2+}$ with a photochemical quantum yield, $\Phi_{NO}$, of 0.086.[55] As shown in Figure 5a, irradiation of **acac-RuNO** in acetonitrile under similar conditions led to a rapid spectral evolution characterized by an increase of the absorbance around $\lambda$ = 500 nm and a decrease of the RuNO band ($\lambda$ = 342 nm). Although growth of the absorbance at $\lambda$ = 500 nm is in agreement with the optical spectrum reported for the expected photoproduct $[Ru(tpy)(acac)(CH_3CN)]^{+}$ [40] and apparent isosbestic points observed around $\lambda$ = 335 and 372 nm suggest a clean conversion to this acetonitrile solvate, gradual loss of these isosbestic points under prolonged irradiation indicates a more complex photochemical reaction. HRMS analysis indicated a nitrated final photoproduct, also observed for other RuNO complexes as illustrated in the Supporting Information (Figures S135-S136). As shown in Figure 5b, this photochemical behavior was largely mirrored by $[Ru^{II}NO(tpy)(acac)](Cl)_2$ (**7a**), the water-soluble analogue of **acac-RuNO**, when irradiated in similar conditions in water. The main difference was that the photoreaction was significantly slower, forcing us to increase the photon flux, $I_0$, by ca. one order of magnitude. Despite several attempts to determine the nature of the photoproduct, no evidence of the expected aqua solvate was obtained.

Although unanticipated, the photoinduced nitration on the acac ligand parallels our previous discussion of an unexpected complex nitrated at the methine position of the acac ligand (*vide supra*). Additionally, being a highly reactive species, it is not uncommon to find nitric oxide participating in this sort of oxidative processes. We have previously reported similar electrophilic additions being promoted on electron-rich aromatic rings[60] as well as nitrates being found as counterions on SXRD analyses of related photoproducts.[59] In spite of the analytical difficulties introduced by this side-reaction, we decided to explore the NO photorelease efficiency of the acac ruthenium nitrosyls; fitting of the photokinetic data for **acac-RuNO** in acetonitrile within the first 20 minutes of irradiation leads to $\Phi_{NO}$ = 0.065 (details in the Supporting Information, Section S7). Although this value seems comparable to that of the **bpy-RuNO** benchmark ($\Phi_{NO}$ = 0.086), it may be significantly underestimated due to the competing nitration, even if the obtained value already highlights a good efficiency for NO delivery in acetonitrile. We must mention that the $\Phi_{NO}$ values for all the acac ruthenium nitrosyls were estimated assuming that the last spectrum in the photokinetics corresponds largely to the non-nitrated photoproduct. We consider this unavoidable assumption reasonable due to (a) the presence of pseudo isosbestic points and small changes in absorption at the determination time, (b) reasonably good fittings of experimental data with the photokinetic model ($R^2 > 0.95$) and (c) the

fact that the observed spectral evolution within the chosen time frame indeed corresponds to NO release as evidenced systematically for all the series using different techniques exemplified in Figures 5c-d.

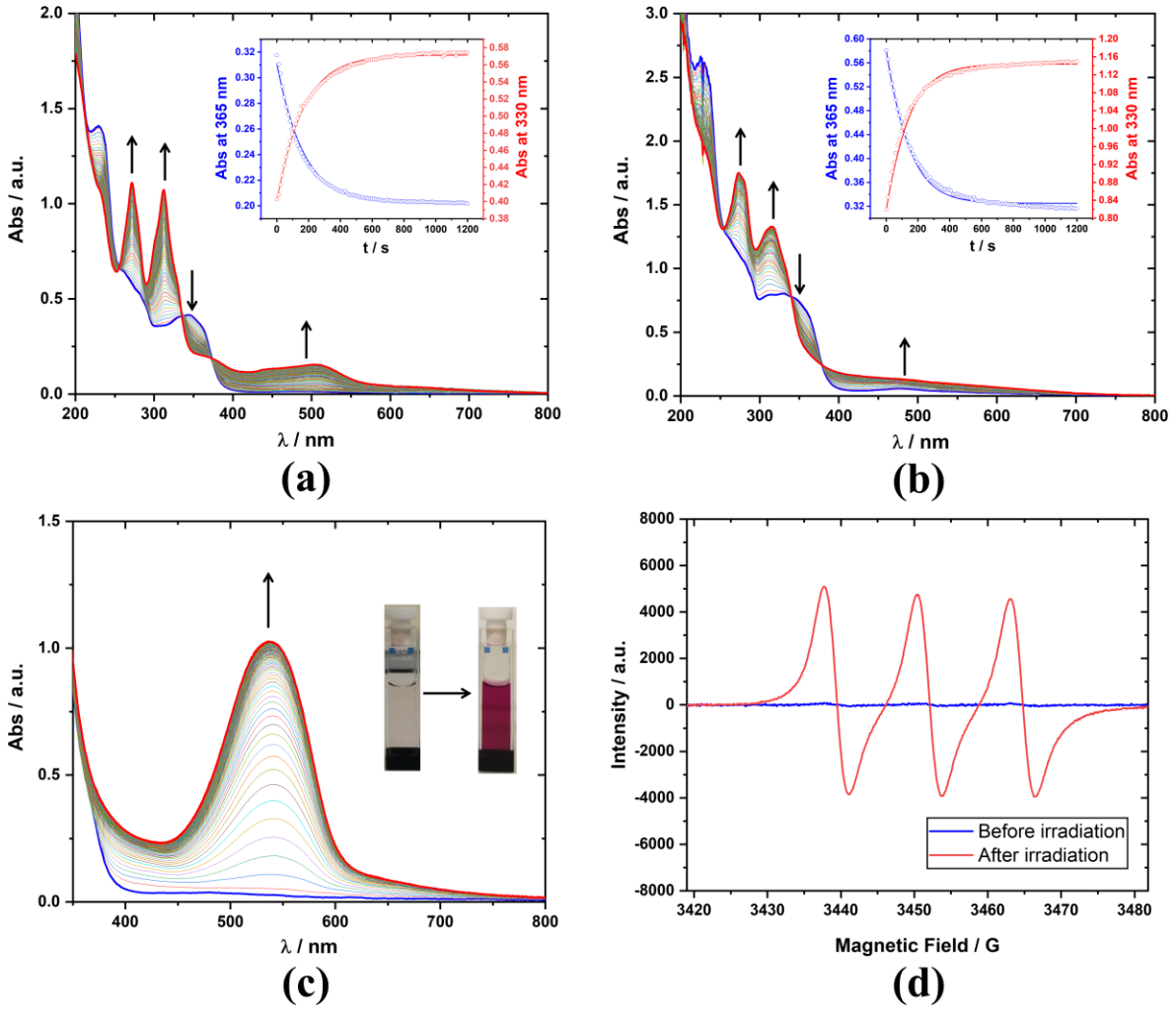


**Figure 5.** Spectral evolution at 25 °C under irradiation at λ = 365 nm during 20 min for (a) **acac-RuNO** (**6a**, 3.54x10$^{-5}$ M in acetonitrile, $I_0$ = 6.22x10$^{-6}$ molL$^{-1}$s$^{-1}$) and (b) **7a** (7.31x10$^{-5}$ M in water, $I_0$ = 6.35x10$^{-5}$ molL$^{-1}$s$^{-1}$); inset shows fitting of the photokinetic data at two wavelengths, with average correlation coefficients $R^2$ = 0.995 and 0.993, respectively. Below are representative experiments on **7a** that demonstrate NO release in water under irradiation at λ = 365 nm, as evidenced from (c) the formation of an azo dye in the presence of the Griess reagent[61] and (d) the observation of an EPR signal using the NO-selective [Fe$^{II}$(MGD)$_2$] spin trap; with a *g*-factor of 2.040 and a hyperfine coupling constant, $a_N$ = 1.20x10$^{-3}$ cm$^{-1}$, the observed triplet EPR signal corresponds to a nitric oxide radical.[62]

Although the photochemistry of metal nitrosyls is most frequently investigated in organic solvents, their intended biological applications naturally require working in aqueous media. This observation highlights a problem of solubility or stability in aqueous media in most systems, such as those encountered for the [Ru$^{II}$NO(tpy)(bpy)]$^{3+}$ family. In the present study, the NO photorelease for

only one complex, **tris-acac-RuNO**, had to be investigated in acetonitrile due to its poor solubility in water (see the Supporting Information, Section S7), while all the other acac RuNO complexes overcame this limitation. Consequently, we extended the investigation of the photorelease efficiency in water to complexes **7a-f** and **7h-m**. With the exception of **7f**, that has an intricated acid-base equilibrium in water and thus require a detailed analysis outside of the scope of this paper, we were able to determine the $\Phi_{NO}$ for this family of complexes which lie in the $\Phi_{NO}$ = 0.008 – 0.021 interval (for details see the Supporting Information, Table S5). A tendency towards higher $\Phi_{NO}$ values for complexes with electron withdrawing groups is apparent but no direct correlation was observed between $\Phi_{NO}$ and the Hammett constant, $\sigma_p^+$, of the different substituents in the phenyl series (for details see the Supporting Information, Figure S22). These difficulties at stablishing correlations between the electron donating/withdrawing character of the terpyridyl ligand and $\Phi_{NO}$, paralleled by previous research from our group,[63] are connected with the complex mechanism behind the Ru-NO photodissociation which is broadly considered to involve a complex series of molecular events including photoisomerization processes and the population of diverse excited states.[64-67] It seems therefore reasonable to find difficulties when trying to correlate such a complex excited state observable with a ground-state descriptor like $\sigma_p^+$.

**Two-Photon Absorption Triggered NO Release**

As previously discussed, one of the main objectives of this work was to demonstrate the possibility of building a NO delivery platform, based on the original $[Ru^{II}NO(tpy)(acac)]^{2+}$ coordination sphere, that could be efficiently activated through a two-photon absorption (TPA) process in aqueous media. TPA-triggered phototherapies bring unique advantages such as a largely unparalleled spatiotemporal control of drug delivery and a maximum penetration in human tissues through the use of far-visible to near-IR light sources. Consequently, we decided to investigate the TPA response of **tris-acac-RuNO** as the most promising candidate among the different complexes under investigation. These measurements had to be undertaken in acetonitrile given the limited solubility of this complex in water. Due to the presence of a $C_3$ symmetry axis along the central phenyl ring, **tris-acac-RuNO** was expected to display a large TPA cross section ($\sigma_{TPA}$). The presence of this symmetry element imparts an octupolar electronic architecture for this complex, resulting from fluorenyl and RuNO moieties acting as strong electron donating and withdrawing groups, respectively. Cooperative interactions among the local dipoles result in large $\sigma_{TPA}$ values being frequently observed for molecules with such highly polarizable architectures.[17-20]

Following the above expectations, the TPA properties of **tris-acac-RuNO** have been evaluated by measuring its $\sigma_{TPA}$ using the open-aperture Z-scan method[68-69] at $\lambda$ = 800 nm. The irradiation wavelength was chosen considering that the NO band of the complex is located at $\lambda$ = 444 nm (see the Supporting Information, Figure S19) and should consequently be accessible by TPA at $\lambda$ = 800 nm. Figure 6a depicts several Z-scan traces of **tris-acac-RuNO** in acetonitrile (0.6 mM) for various incident powers at $\lambda$ = 800 nm. The linear correlation between the variation of transmission ($\Delta$T) and the laser power clearly confirms the dominant two-photon absorption regime.[70] With this respect, it can be derived that **tris-acac-RuNO** exhibits a very high $\sigma_{TPA}$ of about 1530 ± 240 GM at 800 nm.

This significant $\sigma_{TPA}$ value echoes that measured previously for a similar three branched truxene-based complex[27] (~ 1600 GM) which was also decorated with three Ru-NO subunits. The presence of these strong electron withdrawing metal-centers positioned at the rim of a π-conjugated octupole with a $C_3$-symmetry clearly promotes a strong electronic coupling among the individual arms of the molecule giving rise to a very strong NLO response. Such electronic coupling was inspected by DFT in the frontier orbitals of a $C_3$ optimized model of **tris-acacRuNO**, evidencing a significant mixing of the different fluorenyl arms in the lowest-lying occupied levels (orbitals 475-477), exemplified with the HOMO (orbital 475) in Figure 6b, while the nearly degenerate unoccupied levels (orbitals 478-480) remained largely isolated at the individual RuNO cores, as exemplified with the LUMO (orbital 478) in the same Figure.

The observed structure / TPA property relationship has been previously rationalized by Beljonne *et al*.[71] who predicted a strong enhancement of the TPA cross-section of $C_3$-type octupoles into their $S_2$ excited state by modulating the electronic interbranch cross-talk effect. In our case, the choice of Ru-NO complex subunit seems well suited for this molecular engineering strategy since it not only participates the TPA amplification but can also promote a subsequent release of NO molecules upon two-photon excitation. To illustrate this second valuable property, an aqueous solution of **tris-acac-RuNO** was two-photon excited at 800 nm in presence of Griess reagent used as *in situ* NO probe. Figure 6c shows the time-dependent differential absorption spectrum (i.e. $A_t - A_0$) of the mixing solution during the two-photon irradiation. Note that a reference solution of **tris-acac-RuNO** without Griess reagent was also irradiated in the same conditions (Supplementary Figure S36). The comparison of both experiments clearly indicates that the incremental irradiation of the solution of **tris-acac-RuNO** with Griess reagent leads to the progressive release of NO whose presence is highlighted by the growth of absorption bands in the 500-720 nm which typically correspond to the generation of the corresponding azo dye.[57, 72]

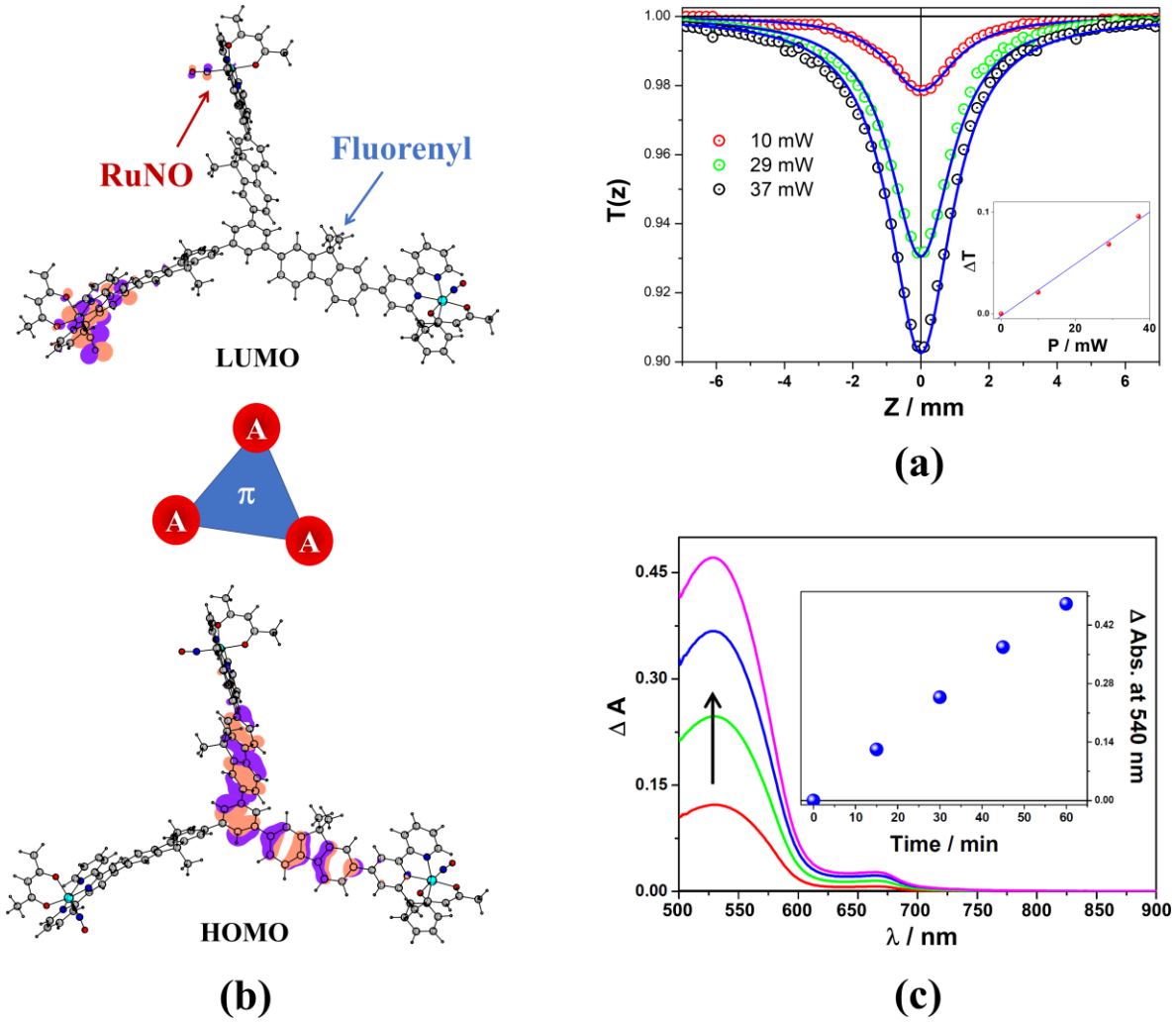


**Figure 6.** Two-photon absorption properties for **tris-acacRuNO**. (a) Z-traces in acetonitrile (0.6 mM) at 800 nm for various incident laser powers. Each Z-trace has been fitted using the model curve detailed in the Supporting Information (Section S8). Inset: Transmittance variation *vs.* excitation power (b) Schematic representation of the octupolar electronic structure and frontier molecular orbitals computed for a molecular model in the $C_3$ symmetry at the CAM-B3LYP/6-31* level in acetonitrile. (c) Time-dependent differential absorption spectra (i.e. $\Delta A = A(t) - A(0)$) in aqueous medium during its two-photon irradiation at 806 nm in presence of the Griess reagent.[61] Inset: ΔA recorded at 540 nm after each 15 min irradiation increment. Solvent: isovolume mixture of ACN/Water, [**tris-acac-RuNO**] = 0.4 mM, µ-volume cuvette with 2 mm optical path, $P_{806nm}$ = 1.02 W.

## CONCLUSION

In this work we tackled the significant instability in water displayed by the $[RuNO(tpy)(bpy)]^{3+}$ family of ruthenium nitrosyls that has precluded their potential phototherapeutic applications as photoactivatable nitric oxide (NO) releasing molecules (photoNORMs). Enhancing the Ru-NO π-backbonding to lower the positive charge at the nitrosyl ligand and thus its susceptibility towards nucleophilic attacks by water or other species was our molecular engineering approach to address this issue. Our strategy consisted in replacing the neutral bipyridine (bpy) for an anionic, electron-rich, acetylacetonate (acac) ligand, yielding $[RuNO(tpy)(acac)]^{2+}$ as a new family of photoNORMs.

Our efforts provided us with a convenient synthetic strategy successfully extrapolated to several mononuclear complexes and to an octupolar star-shaped complex bearing three RuNO moieties (**tris-acac-RuNO**). The impact of the bpy→acac replacement on the electronic, optical and photochemical properties of this novel family of photoNORMs was systematically investigated with support from DFT computations, providing concurring evidence for the expected enhancement of the Ru-NO π-backbonding in these complexes that gratifyingly manifested as a remarkable stability in water during weeks when protected from light. The developed ruthenium nitrosyls were satisfactorily found to release NO in water, although a concomitant nitration of the acac ligand posed analytical difficulties to the precise quantification of the efficiency of the photoreaction. Nonetheless, this competing process should not be regarded as drawback, as targeted biological structures are expected to compete for the released nitric oxide radicals; an indication supporting this hypothesis is found in the efficient trapping by a NO-selective spin trap during photolysis experiments followed by EPR.

Stepping further towards therapeutic applications, in this work we demonstrated that this original coordination sphere permits obtaining sophisticated water-stable multipolar NO-delivery platforms that can be activated in the near-IR region of high biological transparency via a two-photon absorption (TPA) process, as demonstrated for **tris-acac-RuNO** that reached a remarkable TPA cross section of 1530 GM at $\lambda$ = 800 nm and for which NO photorelease was demonstrated under TPA irradiation in aqueous media. Collaborative efforts are currently being undertaken by our group to evaluate the biological activity of this new class of photoNORMs in the context of their potential applications in the treatment of infections from multi-drug resistant bacteria.

## SUPPORTING INFORMATION

Copies of NMR spectra, experimental details and procedures and computational methods are included as Supporting Information (PDF).

## ACKNLOWLEDGMENTS

The authors thank Alain Moreau and Carine Duhayon from LCC for their help recording electrochemical and X-Ray data, respectively, and acknowledge the financial support of CNRS (France). P.L.-V. acknowledges support from the French National Research Agency under program

ANR-18-CE29-0012. This project has received funding through the MSCA4Ukraine project, which is funded by the European Union.

## REFERENCES AND NOTES

1. Shi, H.; Sadler, P. J., How promising is phototherapy for cancer? *Br. J. Cancer* **2020,** *123* (6), 871-873.
2. Karges, J.; Kuang, S.; Maschietto, F.; Blacque, O.; Ciofini, I.; Chao, H.; Gasser, G., Rationally designed ruthenium complexes for 1- and 2-photon photodynamic therapy. *Nat. Commun.* **2020,** *11* (1), 3262.
3. Ortega-Forte, E.; Rovira, A.; López-Corrales, M.; Hernández-García, A.; Ballester, F. J.; Izquierdo-García, E.; Jordà-Redondo, M.; Bosch, M.; Nonell, S.; Santana, M. D.; Ruiz, J.; Marchán, V.; Gasser, G., A near-infrared light-activatable Ru(ii)-coumarin photosensitizer active under hypoxic conditions. *Chem. Sci.* **2023,** *14* (26), 7170-7184.
4. An, J.; Tang, S.; Hong, G.; Chen, W.; Chen, M.; Song, J.; Li, Z.; Peng, X.; Song, F.; Zheng, W.-H., An unexpected strategy to alleviate hypoxia limitation of photodynamic therapy by biotinylation of photosensitizers. *Nat. Commun.* **2022,** *13* (1), 2225.
5. Bian, H.; Ma, D.; Pan, F.; Zhang, X.; Xin, K.; Zhang, X.; Yang, Y.; Peng, X.; Xiao, Y., Cardiolipin-Targeted NIR-II Fluorophore Causes "Avalanche Effects" for Re-Engaging Cancer Apoptosis and Inhibiting Metastasis. *J. Am. Chem. Soc.* **2022,** *144* (49), 22562-22573.
6. Amarsy, I.; Papot, S.; Gasser, G., Stimuli-Responsive Metal Complexes for Biomedical Applications. *Angew. Chem. Int. Ed.* **2022,** *61* (40), e202205900.
7. Farrer, N. J.; Salassa, L.; Sadler, P. J., Photoactivated chemotherapy (PACT): the potential of excited-state d-block metals in medicine. *Dalton Trans.* **2009,** (48), 10690-10701.
8. Bonnet, S., Why develop photoactivated chemotherapy? *Dalton Trans.* **2018,** *47* (31), 10330-10343.
9. Roy, B.; Shieh, M.; Xu, S.; Ni, X.; Xian, M., Single-Component Photo-Responsive Template for the Controlled Release of NO and H2S2. *J. Am. Chem. Soc.* **2023,** *145* (1), 277-287.
10. Möller, M.; Botti, H.; Batthyany, C.; Rubbo, H.; Radi, R.; Denicola, A., Direct Measurement of Nitric Oxide and Oxygen Partitioning into Liposomes and Low Density Lipoprotein*. *J. Biol. Chem.* **2005,** *280* (10), 8850-8854.
11. Figueroa, X. F.; Lillo, M. A.; Gaete, P. S.; Riquelme, M. A.; Sáez, J. C., Diffusion of nitric oxide across cell membranes of the vascular wall requires specific connexin-based channels. *Neuropharmacology* **2013,** *75*, 471-478.
12. Snyder, S. H., Nitric Oxide: First in a New Class of Neurotransmitters. *Science* **1992,** *257* (5069), 494-496.
13. Stamler, J. S.; Singel, D. J.; Loscalzo, J., Biochemistry of Nitric Oxide and Its Redox-Activated Forms. *Science* **1992,** *258* (5090), 1898-1902.
14. Ignarro, L. J., Nitric Oxide: A Unique Endogenous Signaling Molecule in Vascular Biology (Nobel Lecture). *Angew. Chem. Int. Ed.* **1999,** *38* (13-14), 1882-1892.
15. Thomas, D. D.; Ridnour, L. A.; Isenberg, J. S.; Flores-Santana, W.; Switzer, C. H.; Donzelli, S.; Hussain, P.; Vecoli, C.; Paolocci, N.; Ambs, S.; Colton, C. A.; Harris, C. C.; Roberts, D. D.; Wink, D. A., The chemical biology of nitric oxide: Implications in cellular signaling. *Free Radical Biol. Med.* **2008,** *45* (1), 18-31.
16. Girotti, A. W., Tumor-generated nitric oxide as an antagonist of photodynamic therapy. *Photochem. Photobiol. Sci.* **2015,** *14* (8), 1425-1432.
17. Shaw, P. A.; Forsyth, E.; Haseeb, F.; Yang, S.; Bradley, M.; Klausen, M., Two-Photon Absorption: An Open Door to the NIR-II Biological Window? *Front. Chem.* **2022,** *10*.

18. Xu, L.; Zhang, J.; Yin, L.; Long, X.; Zhang, W.; Zhang, Q., Recent progress in efficient organic two-photon dyes for fluorescence imaging and photodynamic therapy. *J. Mater. Chem. C* **2020,** *8* (19), 6342-6349.
19. He, G. S.; Tan, L.-S.; Zheng, Q.; Prasad, P. N., Multiphoton Absorbing Materials: Molecular Designs, Characterizations, and Applications. *Chem. Rev.* **2008,** *108* (4), 1245-1330.
20. Pawlicki, M.; Collins, H. A.; Denning, R. G.; Anderson, H. L., Two-Photon Absorption and the Design of Two-Photon Dyes. *Angew. Chem. Int. Ed.* **2009,** *48* (18), 3244-3266.
21. Samkoe, K.; Clancy, A.; Karotki, A.; Wilson, B.; Cramb, D., Complete blood vessel occlusion in the chick chorioallantoic membrane using two-photon excitation photodynamic therapy: implications for treatment of wet age-related macular degeneration. *J. Biomed. Opt.* **2007,** *12* (3), 034025.
22. Richards-Kortum, R.; Sevick-Muraca, E., QUANTITATIVE OPTICAL SPECTROSCOPY FOR TISSUE DIAGNOSIS. *Annu. Rev. Phys. Chem.* **1996,** *47* (1), 555-606.
23. Bolze, F.; Jenni, S.; Sour, A.; Heitz, V., Molecular photosensitisers for two-photon photodynamic therapy. *Chem. Commun.* **2017,** *53* (96), 12857-12877.
24. Lacroix, P. G.; Malfant, I.; Labra-Vázquez, P.; Fárfan, N.; Ramos-Ortiz, G., Two-photon absorption-based delivery of nitric oxide from ruthenium nitrosyl complexes. *Dalton Trans.* **2022,** *51* (39), 14833-14841.
25. Enriquez-Cabrera, A.; Sasaki, I.; Bukhanko, V.; Tassé, M.; Mallet-Ladeira, S.; Lacroix, P. G.; Barba-Barba, R. M.; Ramos-Ortiz, G.; Farfán, N.; Voitenko, Z.; Malfant, I., Replacing Two Chlorido Ligands by a Bipyridine Ligand in Ruthenium Nitrosyl Complexes with NO-Release Capabilities: A Comparative Study. *Eur. J. Inorg. Chem.* **2017,** *2017* (11), 1446-1456.
26. Juarez-Martinez, Y.; Labra-Vázquez, P.; Enríquez-Cabrera, A.; Leon-Rojas, A. F.; Martínez-Bourget, D.; Lacroix, P. G.; Tassé, M.; Mallet-Ladeira, S.; Farfán, N.; Santillan, R.; Ramos-Ortiz, G.; Malval, J.-P.; Malfant, I., Bimetallic Ruthenium Nitrosyl Complexes with Enhanced Two-Photon Absorption Properties for Nitric Oxide Delivery. *Chem. Eur. J.* **2022,** *28* (62), e202201692.
27. Romero Ávila, M.; León-Rojas, A. F.; Lacroix, P. G.; Malfant, I.; Farfán, N.; Mhanna, R.; Santillan, R.; Ramos-Ortiz, G.; Malval, J.-P., Two-Photon-Triggered NO Release via a Ruthenium–Nitrosyl Complex with a Star-Shaped Architecture. *J. Phys. Chem. Lett.* **2020,** *11* (16), 6487-6491.
28. Christopoulos, K.; Karidi, K.; Tsipis, A.; Garoufis, A., Synthesis, characterization, DNA-binding properties and electronic structure (DFT) of ruthenium oligopyridine complexes. *Inorg. Chem. Commun.* **2008,** *11* (11), 1341-1346.
29. de Lima, R. G.; Sauaia, M. G.; Ferezin, C.; Pepe, I. M.; José, N. M.; Bendhack, L. M.; da Rocha, Z. N.; da Silva, R. S., Photochemical and pharmacological aspects of nitric oxide release from some nitrosyl ruthenium complexes entrapped in sol–gel and silicone matrices. *Polyhedron* **2007,** *26* (16), 4620-4624.
30. Roncaroli, F.; Ruggiero, M. E.; Franco, D. W.; Estiú, G. L.; Olabe, J. A., Kinetic, Mechanistic, and DFT Study of the Electrophilic Reactions of Nitrosyl Complexes with Hydroxide. *Inorg. Chem.* **2002,** *41* (22), 5760-5769.
31. Bocé, M.; Tassé, M.; Mallet-Ladeira, S.; Pillet, F.; Da Silva, C.; Vicendo, P.; Lacroix, P. G.; Malfant, I.; Rols, M.-P., Effect of trans(NO, OH)-[RuFT(Cl)(OH)NO](PF6) ruthenium nitrosyl complex on methicillin-resistant Staphylococcus epidermidis. *Sci. Rep.* **2019,** *9* (1), 4867.
32. Labra-Vázquez, P.; Bocé, M.; Tassé, M.; Mallet-Ladeira, S.; Lacroix, P. G.; Farfán, N.; Malfant, I., Chemical and photochemical behavior of ruthenium nitrosyl complexes with terpyridine ligands in aqueous media. *Dalton Trans.* **2020,** *49* (10), 3138-3154.
33. Olivier, J.-H.; Harrowfield, J.; Ziessel, R., 3-Substituted-2,4-pentanedionates: ligands for photoactive supramolecular assemblies. *Chem. Commun.* **2011,** *47* (40), 11176-11188.
34. Tapparo, A.; Perazzolo, M., N-Octanol/Water Partition Coefficients of the Acetylacetonate and Maltolate Complexes of Al(III), Cr(III) and Fe(III) and of Aluminum Lactate. *Int. J. Environ. Anal. Chem.* **1989,** *36* (1), 13-16.

35. Halverson, F.; Brinen, J. S.; Leto, J. R., Photoluminescence of Lanthanide Complexes. II. Enhancement by an Insulating Sheath. *J. Chem. Phys.* **2004,** *41* (1), 157-163.
36. He, L.; Cao, J.-J.; Zhang, D.-Y.; Hao, L.; Zhang, M.-F.; Tan, C.-P.; Ji, L.-N.; Mao, Z.-W., Lipophilic phosphorescent iridium(III) complexes as one- and two-photon selective bioprobes for lipid droplets imaging in living cells. *Sensors Actuators B: Chem.* **2018,** *262*, 313-325.
37. Lipinski, C. A.; Lombardo, F.; Dominy, B. W.; Feeney, P. J., Experimental and computational approaches to estimate solubility and permeability in drug discovery and development settings. *Adv. Drug Del. Rev.* **1997,** *23* (1), 3-25.
38. Ghose, A. K.; Viswanadhan, V. N.; Wendoloski, J. J., A Knowledge-Based Approach in Designing Combinatorial or Medicinal Chemistry Libraries for Drug Discovery. 1. A Qualitative and Quantitative Characterization of Known Drug Databases. *J. Comb. Chem.* **1999,** *1* (1), 55-68.
39. Dovletoglou, A.; Adeyemi, S. A.; Meyer, T. J., Coordination and Redox Chemistry of Substituted-Polypyridyl Complexes of Ruthenium. *Inorg. Chem.* **1996,** *35* (14), 4120-4127.
40. Loftus, L. M.; Al-Afyouni, K. F.; Turro, C., New RuII Scaffold for Photoinduced Ligand Release with Red Light in the Photodynamic Therapy (PDT) Window. *Chem. Eur. J.* **2018,** *24* (45), 11550-11553.
41. Adeyemi, S. A.; Dovletoglou, A.; Guadalupe, A. R.; Meyer, T. J., Redox and spectral properties of the four-electron oxidant trans-aquadioxo(terpyridine)ruthenium(2+) diperchlorate. *Inorg. Chem.* **1992,** *31* (8), 1375-1383.
42. We would like to clarify here that in some cases the acetonitrile solvates (4a-4m) were obtained with a minor (typically ca. 2-5 %) unidentified redish impurity that can be easily removed using column chromatography; we conducted careful comparisons and the presence of this contaminant at this step has no impact neither in the purity of the final RuNO complex nor in the global synthetic yield. Nevertheless, for clarity purposes in few cases the analytical data presented for these acetonitrile solvates involved chromatographic purification.
43. Hansch, C.; Leo, A.; Taft, R. W., A survey of Hammett substituent constants and resonance and field parameters. *Chem. Rev.* **1991,** *91* (2), 165-195.
44. Roose, M.; Sasaki, I.; Bukhanko, V.; Mallet-Ladeira, S.; Barba-Barba, R. M.; Ramos-Ortiz, G.; Enriquez-Cabrera, A.; Farfán, N.; Lacroix, P. G.; Malfant, I., Nitric oxide photo-release from a ruthenium nitrosyl complex with a 4,4′-bisfluorenyl-2,2′-bipyridine ligand. *Polyhedron* **2018,** *151*, 100-111.
45. Scott, A. P.; Radom, L., Harmonic Vibrational Frequencies: An Evaluation of Hartree−Fock, Møller−Plesset, Quadratic Configuration Interaction, Density Functional Theory, and Semiempirical Scale Factors. *J. Phys. Chem.* **1996,** *100* (41), 16502-16513.
46. Marchenko, N.; Lacroix, P. G.; Bukhanko, V.; Tassé, M.; Duhayon, C.; Boggio-Pasqua, M.; Malfant, I., Multistep Photochemical Reactions of Polypyridine-Based Ruthenium Nitrosyl Complexes in Dimethylsulfoxide. *Molecules* **2020,** *25* (9), 2205.
47. Enemark, J. H.; Feltham, R. D., Principles of structure, bonding, and reactivity for metal nitrosyl complexes. *Coord. Chem. Rev.* **1974,** *13* (4), 339-406.
48. Bader, R. F. W.; MacDougall, P. J.; Lau, C. D. H., Bonded and nonbonded charge concentrations and their relation to molecular geometry and reactivity. *J. Am. Chem. Soc.* **1984,** *106* (6), 1594-1605.
49. Bader, R. F. W.; Essén, H., The characterization of atomic interactions. *J. Chem. Phys.* **1984,** *80* (5), 1943-1960.
50. Espinosa, E.; Molins, E.; Lecomte, C., Hydrogen bond strengths revealed by topological analyses of experimentally observed electron densities. *Chem. Phys. Lett.* **1998,** *285* (3), 170-173.
51. Matta, C. F.; Boyd, R. J., An Introduction to the Quantum Theory of Atoms in Molecules. In *The Quantum Theory of Atoms in Molecules*, 2007; pp 1-34.
52. Labra-Vázquez, P.; Ochoa, M. E.; Alfonso-Herrera, L. A.; Vera, M. A.; Farfán, N.; Santillan, R., A Steroidal Molecular Rotor with Fast Solid-State Dynamics Obtained by Crystal Engineering: Role of the Polarity of the Stator. *Eur. J. Org. Chem.* **2022,** *2022* (38), e202200351.

53. Stepanenko, I.; Mizetskyi, P.; Orlowska, E.; Bučinský, L.; Zalibera, M.; Vénosová, B.; Clémancey, M.; Blondin, G.; Rapta, P.; Novitchi, G.; Schrader, W.; Schaniel, D.; Chen, Y.-S.; Lutz, M.; Kožíšek, J.; Telser, J.; Arion, V. B., The Ruthenium Nitrosyl Moiety in Clusters: Trinuclear Linear μ-Hydroxido Magnesium(II)-Diruthenium(II), μ3-Oxido Trinuclear Diiron(III)–Ruthenium(II), and Tetranuclear μ4-Oxido Trigallium(III)-Ruthenium(II) Complexes. *Inorg. Chem.* **2022,** *61* (2), 950-967.
54. Nelyubina, Y. V.; Lyssenko, K. A.; Kotov, V. Y.; Antipin, M. Y., Anion−Anion Assembly in Crystal of Sodium Nitroprusside. *J. Phys. Chem. A* **2008,** *112* (37), 8790-8796.
55. Roose, M.; Tassé, M.; Lacroix, P. G.; Malfant, I., Nitric oxide (NO) photo-release in a series of ruthenium–nitrosyl complexes: new experimental insights in the search for a comprehensive mechanism. *New J. Chem.* **2019,** *43* (2), 755-767.
56. Poelhsitz, G. V.; Bogado, A. L.; de Souza, G. D.; Rodrigues-Filho, E.; Batista, A. A.; de Araujo, M. P., New nitrosyl ruthenium complex [RuCl(NO)(dcype)(bipy)](PF6)2: Synthesis, electrochemistry, NMR and ESI-MS/MS studies. *Inorg. Chem. Commun.* **2007,** *10* (2), 133-138.
57. Akl, J.; Sasaki, I.; Lacroix, P. G.; Malfant, I.; Mallet-Ladeira, S.; Vicendo, P.; Farfán, N.; Santillan, R., Comparative photo-release of nitric oxide from isomers of substituted terpyridinenitrosylruthenium(ii) complexes: experimental and computational investigations. *Dalton Trans.* **2014,** *43* (33), 12721-12733.
58. Enríquez-Cabrera, A.; Vega-Peñaloza, A.; Álvarez-Venicio, V.; Romero-Ávila, M.; Lacroix, P. G.; Ramos-Ortiz, G.; Santillan, R.; Farfán, N., Two-photon absorption properties of four new pentacoordinated diorganotin complexes derived from Schiff bases with fluorene. *J. Organomet. Chem.* **2018,** *855*, 51-58.
59. Bukhanko, V.; Lacroix, P. G.; Sasaki, I.; Tassé, M.; Mallet-Ladeira, S.; Voitenko, Z.; Malfant, I., Mechanism and oxidation state involved in the nitric oxide (NO) photorelease in a terpyridine-bipyridine-based ruthenium nitrosyl complex. *Inorg. Chim. Acta* **2018,** *482*, 195-205.
60. Sasaki, I.; Amabilino, S.; Mallet-Ladeira, S.; Tassé, M.; Sournia-Saquet, A.; Lacroix, P. G.; Malfant, I., Further studies on the photoreactivities of ruthenium–nitrosyl complexes with terpyridyl ligands. *New J. Chem.* **2019,** *43* (28), 11241-11250.
61. Tsikas, D., Analysis of nitrite and nitrate in biological fluids by assays based on the Griess reaction: appraisal of the Griess reaction in the L-arginine/nitric oxide area of research. *J. Chromatogr. B: Anal. Technol. Biomed. Life Sci.* **2007,** *851* (1-2), 51-70.
62. Liu, J.; Duan, Q.; Wang, J.; Song, Z.; Qiao, X.; Wang, H., Photocontrolled nitric oxide release from two nitrosylruthenium isomer complexes and their potential biomedical applications. *J. Biomed. Opt.* **2015,** *20* (1), 015004.
63. Amabilino, S.; Tasse, M.; Lacroix, P. G.; Mallet-Ladeira, S.; Pimienta, V.; Akl, J.; Sasaki, I.; Malfant, I., Photorelease of nitric oxide (NO) on ruthenium nitrosyl complexes with phenyl substituted terpyridines. *New J. Chem.* **2017,** *41* (15), 7371-7383.
64. Talotta, F.; González, L.; Boggio-Pasqua, M., CASPT2 Potential Energy Curves for NO Dissociation in a Ruthenium Nitrosyl Complex. *Molecules* **2020,** *25* (11), 2613.
65. Talotta, F.; Heully, J.-L.; Alary, F.; Dixon, I. M.; González, L.; Boggio-Pasqua, M., Linkage Photoisomerization Mechanism in a Photochromic Ruthenium Nitrosyl Complex: New Insights from an MS-CASPT2 Study. *J. Chem. Theory Comput.* **2017,** *13* (12), 6120-6130.
66. Sanz García, J.; Talotta, F.; Alary, F.; Dixon, I. M.; Heully, J.-L.; Boggio-Pasqua, M., A Theoretical Study of the N to O Linkage Photoisomerization Efficiency in a Series of Ruthenium Mononitrosyl Complexes. *Molecules* **2017,** *22* (10), 1667.
67. García, J. S.; Alary, F.; Boggio-Pasqua, M.; Dixon, I. M.; Heully, J.-L., Is photoisomerization required for NO photorelease in ruthenium nitrosyl complexes? *J. Mol. Model.* **2016,** *22* (11), 284.
68. Sheik-bahae, M.; Said, A. A.; Van Stryland, E. W., High-sensitivity, single-beam n2 measurements. *Opt. Lett.* **1989,** *14* (17), 955-957.

69. Sheik-Bahae, M.; Said, A. A.; Wei, T. H.; Hagan, D. J.; Stryland, E. W. V., Sensitive measurement of optical nonlinearities using a single beam. *IEEE J. Quantum Electron.* **1990,** *26* (4), 760-769.
70. Stryland, E. W. V.; Sheik-Bahae, M., Z-Scan Measurements of Optical Nonlinearities. In *Characterization Techniques and Tabulations for Organic Nonlinear Materials*, Kuzyk, M. G.; Dirk, C. W., Eds. Marcel Dekker, Inc.,: 1998; pp 655-692.
71. Beljonne, D.; Wenseleers, W.; Zojer, E.; Shuai, Z.; Vogel, H.; Pond, S. J. K.; Perry, J. W.; Marder, S. R.; Brédas, J.-L., Role of Dimensionality on the Two-Photon Absorption Response of Conjugated Molecules: The Case of Octupolar Compounds. *Adv. Funct. Mater.* **2002,** *12* (9), 631-641.
72. Akl, J.; Sasaki, I.; Lacroix, P. G.; Hugues, V.; Vicendo, P.; Bocé, M.; Mallet-Ladeira, S.; Blanchard-Desce, M.; Malfant, I., trans- and cis-(Cl,Cl)-[RuII(FT)Cl2(NO)](PF6): promising candidates for NO release in the NIR region. *Photochem. Photobiol. Sci.* **2016,** *15* (12), 1484-1491.

**For Table-of-Contents use only**

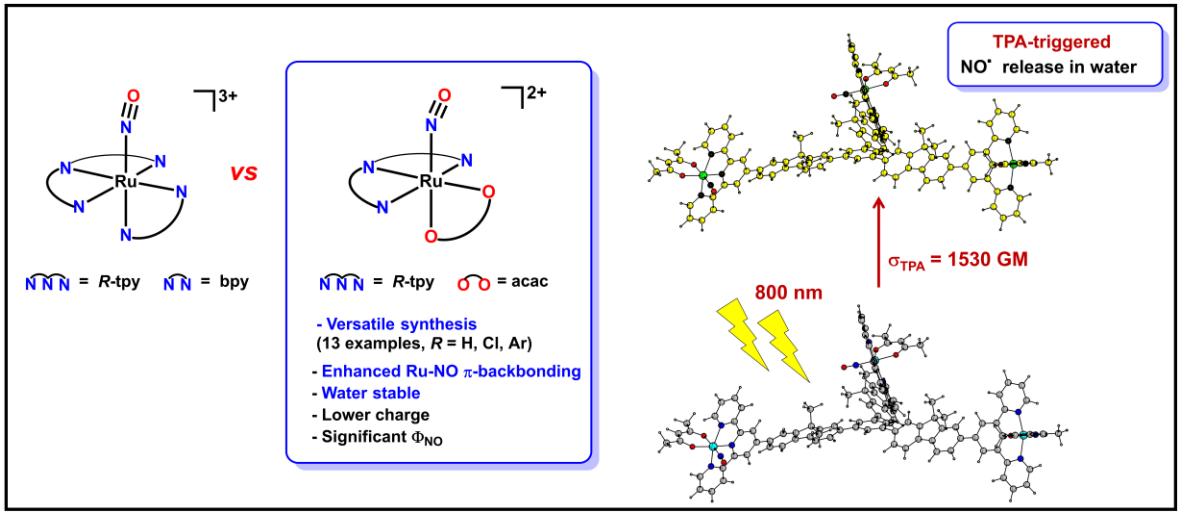


## Synopsis

A novel family of ruthenium nitrosyl complexes for applications in photoactivated chemotherapy is presented. Replacing the commonly employed 2,2'-bipyridine (bpy) ligand for an acetylacetonate (acac) led to an enhanced Ru-NO π-backbonding and thus to high stability in water, where these complexes release nitric oxide (NO) under irradiation. Photoactivation in the near-IR region by two-photon absorption (TPA) is demonstrated for an octupolar complex with a TPA cross section of 1530 GM at λ = 800 nm.